We are IntechOpen, the world's leading publisher of Open Access books Built by scientists, for scientists

4,800
Open access books available

122,000
International authors and editors

135M
Downloads

Our authors are among the

154
Countries delivered to

TOP 1%
most cited scientists

12.2%
Contributors from top 500 universities

WEB OF SCIENCE™

Selection of our books indexed in the Book Citation Index in Web of Science™ Core Collection (BKCI)

Interested in publishing with us?
Contact book.department@intechopen.com

Numbers displayed above are based on latest data collected.
For more information visit www.intechopen.com

Chapter 17

Laser Spectroscopy in Hollow-Core Fibers: Principles and Applications

Philip G. Westergaard

Additional information is available at the end of the chapter

http://dx.doi.org/10.5772/63536

Abstract

The development of hollow-core photonic crystal fiber (HC-PCF) technology over the past decade has opened up a vast array of possibilities for new applications. When the hollow core is filled with gas, the HC-PCF is ideal for molecular spectroscopy applications that require long path length interaction. When light is coupled into the HC-PCF, the overlap between light and the molecules inside the hollow core is excellent all along the length of the fiber, which can be hundreds of meters long. Coiling the fiber up provides a compact, low-weight gas cell at the same time featuring a high level of interaction between laser light coupled through the fiber and the molecules inside.

This chapter presents some theoretical background, different applications, and selected results for molecular spectroscopy using gas-filled hollow-core fibers. The applications include frequency stabilization of a laser to a molecular transition and stimulated Raman scattering in a hollow-core fiber.

Keywords: photonic crystal fiber, hollow-core, HC-PCF, CO2, laser stabilization, stimulated Raman scattering

1. Introduction

Spectroscopy of weak molecular lines or weak scattering processes (such Raman scattering) is typically troubled by a small signal strength caused by insufficient interaction length or optical power, depending on the type of spectroscopy. One possible solution is to use multipass cells for an effective interaction length of up to a few hundred meters. Another, more compact solution is to fill gas into the hollow core of specially designed optical fibers —the so-called hollow-core photonic crystal fibers (HC-PCFs). Here, an interaction length of

INTECH
open science | open minds

© 2016 The Author(s). Licensee InTech. This chapter is distributed under the terms of the Creative Commons Attribution License (http://creativecommons.org/licenses/by/3.0), which permits unrestricted use, distribution, and reproduction in any medium, provided the original work is properly cited.

more than 100 m can be coiled up to a diameter of less than 10 cm. The hollow core ranges from around 10 to 100 microns in diameter, thus providing high intensity of the probe light propagating through the fiber and interacting with the molecules confined to the hollow core inside the fiber.

Applications of gas-filled HC-PCFs include high-accuracy laser stabilization, which can be useful in determining, e.g., the CO_2 content in the atmosphere using remote sensing techniques. These sensing techniques require stabilized laser systems for optimum sensitivity, and using a gas-filled HC-PCF for spectroscopy to stabilize the laser frequency is well suited for this purpose.

Hollow-core fibers with their high optical intensity inside the hollow core and long interaction length are also well suited for observing weak processes such as Raman scattering. This can be carried out by either observing the spontaneously generated stokes light at the output of the fiber, or by stimulating the Raman transition coherently using two input laser beams. Stimulating the Raman transition gives orders of magnitude higher signal and a possibility for higher spectral resolution.

2. Hollow-core fibers

2.1. Guiding light through a hollow core

Conventional optical fibers developed in the beginning of the 1970s [1] guide light inside a core with higher index of refraction than the surrounding layers (the cladding). These fibers are known as step index fibers and guide the light via classical refraction mechanisms such as total internal reflection.

In the beginning of the 1990s, a new technique for guiding light was envisioned [2]. Instead of relying on the mechanism that results from Maxwell's equations for the interface between two infinite mediums, this new technique exploits the constraints on the propagation of the electromagnetic field that arises from a periodic lattice structure of varying index of refraction. This lattice—or crystal—structure gives rise to a band gap in the energy spectrum in which light cannot propagate. This effect is also known from solid-state physics where it is observed for electrons in various periodic structures such as metals and semiconductors. By introducing a regular pattern of tiny holes in the silica structure that makes up a regular fiber (see **Figure 1**, left), an effective lattice pattern emerges and the light will be guided inside the lattice structure according to the band gap equations.

Most notably, it became possible to guide light in a central large hole inside the fiber instead of in a high index medium. This type of fiber is called hollow-core photonic crystal fiber (HC-PCF) and a first realization of this type was produced in 1999 [3]. Confining light in free space (as opposed to a solid core) with surrounding silica structure meant that now it was possible to fill molecules into this central empty part of the fiber and have the light interact with these molecules as it traverses the length of the fiber. This has several advantages. Since the central hollow core has a diameter of typically 10–20 microns[1] depending on the type (**Figure 1**), the

mode of the guided light (which has a shape close to Gaussian) will have a waist diameter around the same size as the core diameter. Such small waists give high intensity of the light, and not just in a small focused spot limited to the corresponding Rayleigh length for Gaussian beams ($\pi w_0^2/\lambda$, where w_0 is the waist radius and λ the wavelength of the light), but over the entire length of the fiber. One can imagine that this potentially allows for a very high degree of interaction between the molecules and the light.

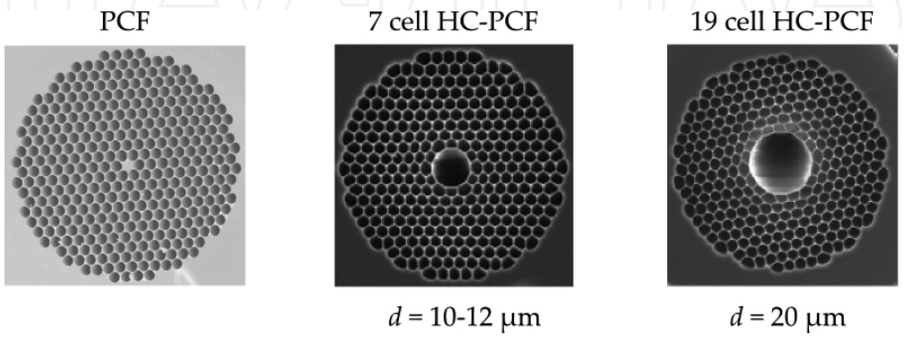

Figure 1. Different examples of photonic crystal fibers. The figure shows microscope images of the fiber tips. Left: A solid-core fiber with a periodic lattice structure of small holes. Middle: The seven-cell HC-PCF has a large central hole where seven rods that comprise the surrounding small holes have been removed. Similarly for the 19 cell HC-PCF (right).

For applications that require compact and lightweight components, such as operation in space, the HC-PCF is an excellent alternative to a bulky glass cell.

2.2. Filling and coupling

When light is transmitted through the HC-PCF, it interacts with the molecules that happen to be situated inside the hollow core. If interaction with molecules other than air is desired, the core of the HC-PCF should first be evacuated and then filled with the molecules of choice. This is done by mounting the fiber ends (or the entire fiber) inside a vacuum system. The vacuum system should also allow optical access for coupling light into the fiber. This is not easily achieved but various techniques exist. If the fiber ends are not enclosed in a vacuum system at all times, the HC-PCF must be sealed in some way to keep the desired molecules inside the fiber.

Basically, two techniques have been used in the literature to seal the gas-filled HC-PCFs. The first technique is based on splicing the ends to standard single-mode fibers. This is relatively easy to do for one end of the HC-PCF before the gas filling, but the single-ended filling time will be rather large for long fibers. Furthermore, Fresnel reflections at the splice interface between the two fibers often introduce interference effects that can affect the transmission properties of the fiber in an unpredictable way [4]. Losses at the splice interface due to mode mismatch can be significant [5], in particular for a (nearly) single-mode HC-PCF. It is also

[1] Other types of hollow-core fibers, such as the Kagomé type, can have several times larger core diameters. These types of fibers will not be discussed here.

possible to splice the HC-PCF to a single-mode fiber after gas filling as demonstrated in [6]. Here, the gas filling is followed by filling with He gas at high pressure (above 1 atm). The high He pressure prevents air from entering the HC-PCF during the splice process. Subsequently, He escapes by diffusion through the HC-PCF silica. With both ends of the HC-PCF spliced to single-mode fiber, strong interference fringes are generally seen due to Fresnel reflections at both splice interfaces [6, 7]. It has been shown that these interferences can be suppressed by angling one splice [7, 8]. However, this technique increases losses, is not yet robust or very reproducible and is susceptible to gas leaks and contamination [7].

An alternative technique uses a compact bulk cell around one or both ends of the HC-PCF [9, 10]. **Figure 2** shows a design recently developed at Danish Fundamental Metrology (DFM) [11] that allows for a compact solution for both coupling of the light and gas filling into the fiber in the same device.

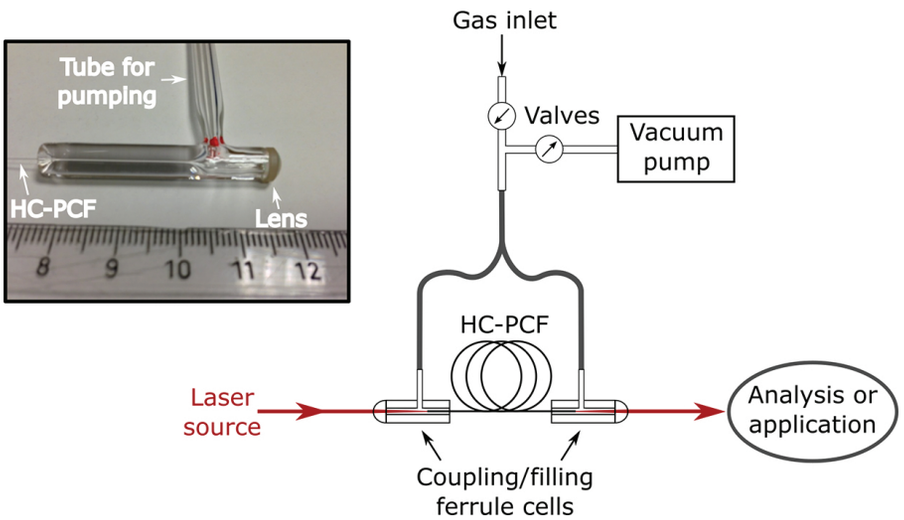

Figure 2. Schematic overview of filling and coupling of the HC-PCF. The hollow core in the fiber must first be evacuated with a vacuum pump, and then it can be filled with a gas. Inset: The ferrule design used for gas filling and coupling light into the HC-PCF. The HC-PCF is inserted into the ferrule from the left and a lens is glued on the right. Evacuating and filling of the hollow core is attained through the tube connected from the top.

In the DFM design, the HC-PCF is inserted into the back of a glass ferrule and is glued in place to avoid leaks and misalignment. The ferrule has a lens glued to the front face for optical coupling, that is, focusing the input light into the core of the HC-PCF. The cell is evacuated and filled with gas via a second smaller tube attached to the side of the outer tube. The cell is sealed off from the pump and filling system after it has been filled with the desired gas. The output of the compact glass cell can be coupled into a single-mode fiber using standard fiber coupling optics.

When the HC-PCF has been set up for gas filling, the system is first evacuated for an extended period, usually several days. After that the system is filled with the relevant gas, which enters the fiber by diffusion. The filling time in the hydrodynamic regime, which is the regime for

the relevant gas pressures used here, can be calculated from molecular parameters and fiber geometry as [12]

$$g_V\left(f, f_0, p, T, m_i\right) = \frac{\sqrt{\frac{\ln(2)}{\pi}}\mathrm{Re}\left(\exp\left(-z^2\right)\mathrm{erfc}\left(-iz\right)\right)}{\Delta f_D}, \tag{1}$$

Considering filling with CO_2 molecules as an example, typical parameters are fiber lengths of up to L = 100 m, d = 10 μm (HC-PCF core diameter), $p_0 \simeq 100$ hPa (gas pressure), and η = $1.50 \cdot 10^{-5}$ kg/(m·s) (CO_2 gas viscosity). The filling time is then calculated to be 28 days. This assumes filling from both ends of the fiber. If the fiber is only filled from one end, the filling time will be four times longer (112 days).

The actual filling time does have some uncertainty. First, it can be reduced by starting with a somewhat higher pressure and then lowering the pressure in the vacuum system to the final pressure at the end of the filling period. It has previously been shown that in the low-pressure regime, the filling time can be reduced to one-sixth of t_{fill} in Eq. (1) by starting out with a pressure 20 times higher than the final pressure [13]. On the other hand, CO_2 tends to adsorb to glass surfaces, and this may increase the filling time [14].

Since the fiber length enters as L^2 in Eq. (1), the filling time can be reduced significantly by reducing the fiber length. Typically, a trade-off between filling time and signal strength must be considered.

3. Spectroscopic applications for laser stabilization

3.1. Molecular absorption

Spectroscopy necessarily relies on the absorption of light by the molecules that are investigated. The amount of absorption depends on molecular parameters (line strength, pressure and velocity distribution), laser parameters (frequency and in some cases optical power), and the interaction length between light and molecules. Power-dependent absorption involves a nonlinear process, such as Raman excitation, which is discussed in Section 4.

When the molecules are held at a given temperature T, their velocity distribution will be given by the Maxwell-Boltzmann equation. Through the Doppler effect, molecules with different velocities will absorb light at different frequencies. This affects the molecular line profile, that is, the absorption (or, correspondingly, the transmission) as a function of laser frequency. Even at zero velocity, the molecular line has a natural profile—the Lorentz profile. When the molecules are moving due to finite temperature, the Lorentz profile is changed into a so-called Voigt profile which is broader and has less absorption on resonance. The effect is illustrated in **Figure 3** where a CO_2 transition at 2051 nm is plotted for different temperatures. For zero temperature, the line profile is Lorentzian.

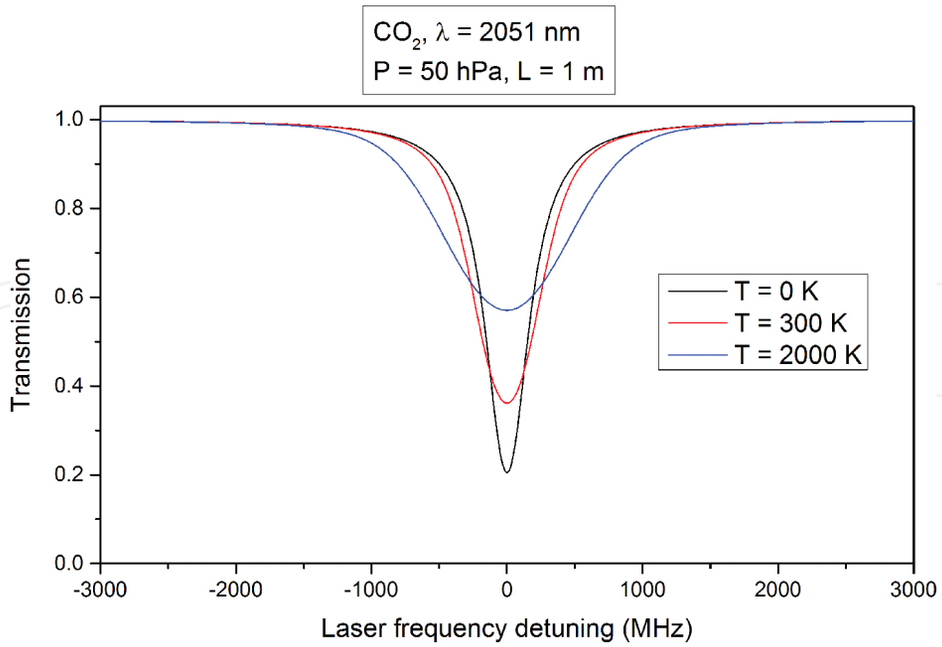

Figure 3. The line profile as a function of laser frequency detuning from molecular resonance for different temperatures of the molecular sample, in this case CO_2 at 50 hPa pressure and 1 m interaction length. The line is broadened by thermal motion at increasing temperatures due to the Doppler effect. The line strength of the transition shown here is 1.504×10^{-22} cm/molecule.

Considering normal excitation of a molecular transition, the amount of absorption can be quantified by the absorption coefficient α_i given by [15]

$$\alpha_i(f, f_0, p, T, m_i) = N(p) \cdot S_i \cdot g_V(f, f_0, p, T, m_i), \tag{2}$$

where i denotes the molecular species, p is the pressure, T is the temperature, f is the laser frequency, f_0 is the center frequency of the molecular line and m_i is the mass of the molecule. $N(p)$ is the number of molecules per volume, given by the ideal gas law $N(p) = \frac{p}{k_B T}$, with k_B being the Boltzmann constant. S_i is the line strength of the transition given in SI units, $[S_i]$ = m²Hz. In the literature, the line strength is often given in units of [cm/molecule]. The relation between the value $S_{i,c}$ in units of [cm/molecule] and the SI line strength $S_{i,c}$ is given by [15]

$$S_i = cS_{i,c}$$

with c being the speed of light.

The factor $g_V(f, f_0, p, T, m_i)$ in Eq. (2) accounts for the Voigt profile of the transition and is given on resonance by [15]

$$g_V\left(f,f_0,p,T,m_i\right)=\frac{\sqrt{\frac{\ln(2)}{\pi}}\mathrm{Re}\left(\exp\left(-z^2\right)\mathrm{erfc}\left(-iz\right)\right)}{\Delta f_D}, \tag{3}$$

where $z=-x+iy$ with $x=\sqrt{\ln(2)}\frac{f-f_0}{\Delta f_D}$ and $y=p\frac{\mathrm{PBC}(p)}{\Delta f_D}\sqrt{\ln(2)}$ with PBC(p) being the pressure broadening coefficient for a pressure p and $\Delta f_D=\frac{f_0}{c}\sqrt{\frac{2\ln(2)k_BT}{m_i}}$ is the Doppler width of the transition. The function erfc(y) is the complex complementary error function.

Equations (2) and (3) can be used to calculate the absorption profile of an arbitrary molecular gas if the line strength, pressure, temperature, and pressure-broadening coefficient are known. In the following section, we will see how this is applied to laser frequency stabilization to a molecular transition.

3.2. Modulation spectroscopy and frequency stabilization

Being an indispensable prerequisite for high-performance remote sensing such as LIDAR (see Section 3.3), frequency stabilization of the laser used for the sensing measurement hinges upon a frequency discriminator that serves as reference for the "correct" value of the laser frequency. Typically, the discriminator is composed of an optical cavity, an atomic line, or—as in the case of molecular sensing—a molecular transition.

Once a suitable frequency discriminator is found, stabilization (otherwise known as locking) of the laser frequency to this reference is accomplished by generation of an electronic signal, known as the error signal, which can be used to steer the laser frequency toward the desired frequency—the laser is then locked. The error signal typically has a large slope around the reference (cavity, molecular, or other) resonance and changes sign when the laser frequency crosses the resonance. This is useful when designing simple electronic circuits (typically PID circuits) that can be used for controlling the laser frequency and locking it to the reference resonance. The standard approach to generate the error signal is by modulation and subsequent demodulation of the laser frequency or phase after the laser light has interacted with the discriminator reference. There are several ways of doing this. In the following section, the frequency modulation spectroscopy (FMS) approach will be discussed for the case of laser frequency stabilization to a molecular transition.

3.2.1. Frequency modulation spectroscopy error signal

For a given set of parameters, the error signal can be simulated from the Voigt profile (Eq. (2)) of the molecular transition. Here, we consider phase modulation of the light and subsequent demodulation to obtain an error signal.

To phase modulate laser light an electro-optic modulator is the most common choice. To see how this affects the light, we consider the electric field component E of the light, which can be

written in complex notation as $E = E_0 e^{i\omega t}$ where ω is the (angular) frequency of the light and E_0 is the amplitude. After modulation, the field becomes (to first order in the Bessel expansion)

$$E_{mod} = E_0 e^{i(\omega t - \beta \sin(\Omega t))} \cong E_0 \left(J_0(\beta) e^{i\omega t} + J_1(\beta) e^{i(\omega+\Omega)t} - J_1(\beta) e^{i(\omega-\Omega)t} \right), \tag{4}$$

where Ω is the modulation (angular) frequency, β is the phase modulation index, and $J_n(\beta)$ is the Bessel function of order n. Spectrally, the laser light is now composed of three components; the carrier at frequency ω and two modulation sidebands at $\omega \pm \Omega$. After the light has passed through the molecular gas (which is here acting as the frequency discriminator), it will have experienced absorption and a phase shift, which both depend on the frequency ω of the light. Introducing the amplitude coefficient of absorption $\alpha_E(\omega)$, the field after passing through the molecular gas becomes[2]

$$E_{out} = E_0 \left[J_0(\beta) e^{i\omega t - \alpha_E(\omega) l} + J_1(\beta) e^{i(\omega+\Omega)t - \alpha_E(\omega+\Omega) l} - J_1(\beta) e^{i(\omega-\Omega)t - \alpha_E(\omega-\Omega) l} \right], \tag{5}$$

where l is the length of the interaction.

When detecting the light, the quantity measured is the intensity $I \propto |E_{out}|^2$. After detection, the signal is demodulated by mixing (multiplying) the measured signal with the modulation signal and low-pass filtering the mixed output to get a DC error signal. Thus, with the field in Eq. (5), the DC error signal becomes after some algebra

$$\mathrm{Err}(\omega, \Omega, \beta) = \frac{\Omega}{2\pi} \int_0^{\frac{2\pi}{\Omega}} \kappa \sin(\Omega t) |E_{out}|^2 \, \mathrm{d}t = \chi e^{-\alpha_E(\omega) l} \left(e^{-\alpha_E(\omega+\Omega) l} - e^{-\alpha_E(\omega-\Omega) l} \right) \tag{6}$$

where $\chi = \kappa {E_0}^2 J_0(\beta) J_1(\beta)$ and κ is the quantum efficiency of the detector. We note that $\alpha_E(\omega)$ is the absorption coefficient for the field amplitude and that the transmission $T_r(\omega) = e^{-\alpha_i(\omega) l}$ through the gas is measured for the intensity of the light using α_i from Eq. (2). The two quantities can be related to via the relation

[2] Here, we neglect the phase shift imparted on the light by the molecules. For typical parameters, this phase shift will be very small and have a negligible contribution to the error signal. For a thermal ensemble, molecules with oppositely directed velocities will contribute equally to the absorption but their contribution to the phase shift will cancel each other out.

$$e^{-\alpha_E(\omega)l} = \sqrt{T_r(\omega)} = \sqrt{e^{-\alpha_i(\omega)l}}. \tag{7}$$

Now, we can model the error signal[3] by inserting Eqs. (2), (3), and (7) in Eq. (6). The transmission $T_r(\omega)$ and the corresponding error signal is shown in **Figure 4** for a CO_2 transition at 2051 nm with a pressure of 5 hPa and 10 m interaction length.

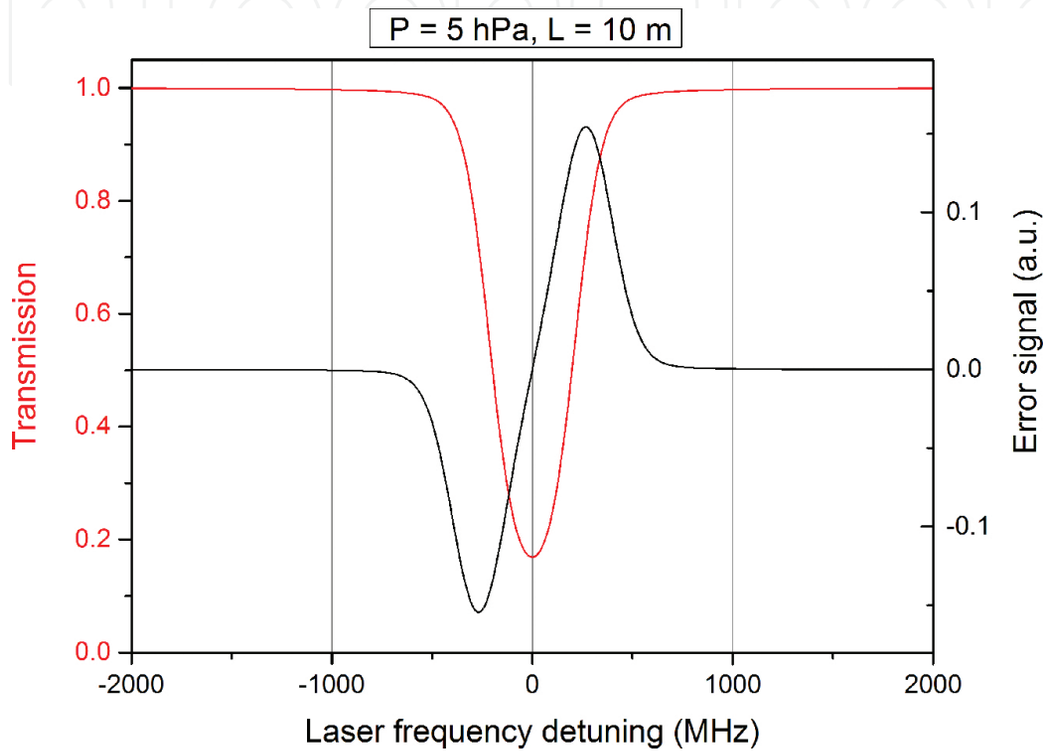

Figure 4. Modeled transmission (red, left scale) and error signal (black, right scale) calculated from Eqs. (2), (3), (6), and (7) for a CO_2 transition at 2051 nm with a pressure of 5 hPa and 10 m interaction length.

The thing to note here is the very linear behavior and zero crossing of the error signal around resonance (i.e., zero detuning). This is ideal as input to an electronic locking mechanism, such as a PID circuit. The long interaction length required to get a large error signal can be difficult to obtain and/or bulky with standard single- or multipass cells. Here, the HC-PCF is ideal as a gas container, since it can have lengths of up to 100 m while being very compact and light weight.

3.3. Applications in remote sensing (LIDAR, DIAL)

The principle of remote sensing (or LIDAR, from LIght Detection And Ranging) using a laser is shown in **Figure 5**. Here, a laser beam is sent through the molecular gas under test and the

[3] In the model presented, here, we do not take into account power broadening because usual power levels are much smaller than the typical saturation power.

absorption from scattered light is detected. For atmospheric sensing the laser source can be satellite based. Important molecules in this respect include the greenhouse gasses CO_2, CH_4, and N_2O.

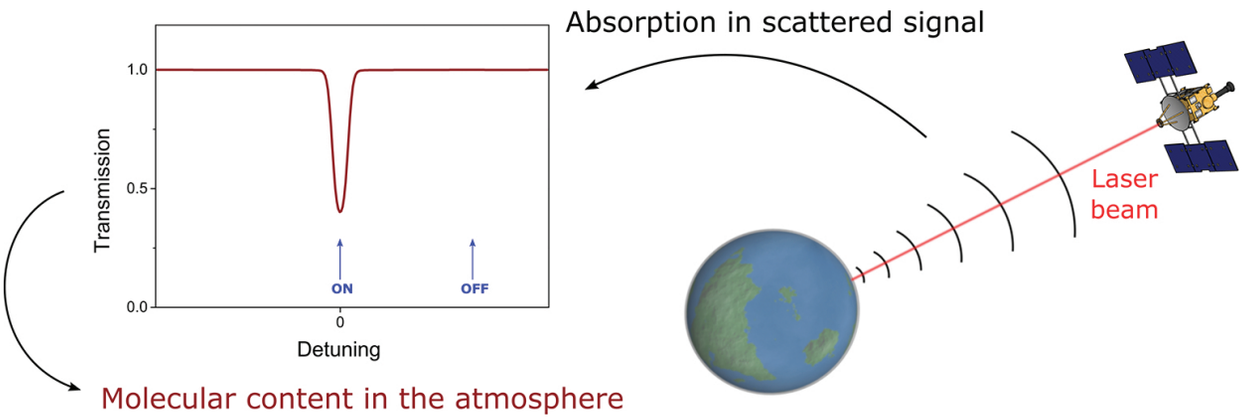

Figure 5. The principle of satellite-based differential atmospheric sensing using LIDAR.

Depending on where the laser frequency is tuned with respect to the molecular transition, the light will experience some absorption by the molecules. If the laser detuning from resonance is well known, this absorption can be directly related to the molecular concentration in the sample gas ($N(p)$ in Eq. (2)). Typically, the laser transmission on resonance (or close to it) is compared to an "off" frequency, where absorption is negligible, which serves as a reference background signal. This differential approach—usually known as DIAL (DIfferential Absorption Lidar)—is one of the most accurate for determining absolute concentrations of molecules in the atmosphere.

One of the main factors determining the accuracy and reliability of the DIAL technique is the frequency stability of the laser used for the absorption measurements. If the laser frequency drifts, the absorption from the molecular transition will change and give an error in the determination of the molecular concentration. Frequency stability down to the level of ±0.3 MHz may be necessary to achieve sufficient accuracy for CO_2 measurements [16]. Most free-running (i.e., not stabilized) laser sources show frequency fluctuations and drift on the order of tens or even hundreds of MHz over the course of minutes to hours. It is thus imperative to lock the laser frequency to a known reference when doing DIAL measurements.

Setting the "on" frequency to the exact center of the molecular resonance does not provide the best possible sensitivity, however. Detecting the transmission at the slope of the transmission curve will give a much higher sensitivity to changes in concentration (see, e.g., **Figure 4**), since pressure-broadening effects render this position highly sensitive to pressure/concentration changes. Therefore, it is desirable to have the possibility to lock the laser "on" frequency at a fixed detuning from the molecular resonance. This can either be performed with additional slave lasers or with just a single laser [17]. For satellite-based operation, it is advantageous to reduce the weight and size of the laser system, and a single laser locked off resonance is preferable if the laser can live up to the stability requirements.

In recent years, efforts have been carried out to obtain sufficiently stable satellite-based laser sources for CO_2 measurements. Among others, NASA has realized stabilization of a fiber-coupled DBF laser to the 1572.3 nm line of CO_2 using a multipass cell [18, 19]. The stability obtained here was at the level of 5.7 kHz up to 1000 s integration time. In the interest of probing atmospheric CO_2 with a wide tuning range about the line center, six DFB slave lasers were offset locked to the master laser at different offsets, and the output light was switched in pulses between the six different slaves. Of course, this type of setup can be bulky and heavy and the large number of components drives up the costs.

To reduce the size and weight, instead of using a multi-pass cell, in 2010 a fiber-coupled Tm:Ho:YLF laser was stabilized to the line center of the CO_2 transition at 2051 nm using a CO_2-filled 10 m long HC-PCF [20]. The resulting standard deviation of the locked frequency was at the level of 2.4 MHz. Also, acetylene and iodine have been used in hollow-core fibers for frequency stabilization, mostly using saturated absorption spectroscopy which can give a more accurate and stable lock, but less opportunity for tuning of the frequency. The most recent experiments report a long-term stability of around 800 Hz [4, 21].

Recently, [17], a compact system was demonstrated using a 10 m HC-PCF for stabilization of a DFB laser to CO_2 at 2051 nm. The setup was designed to be compact and lightweight. This included offset locking away from resonance with just a single laser. **Figure 6** shows experimental data of the transmission and error signal from a 10 m long HC-PCF filled with CO_2 to a pressure of around 20 hPa.

The HC-PCF in [17] was coiled up to a diameter of 8 cm on a copper mount. The control software developed for this system features an automated calibration sequence, which makes it possible to achieve an accurate and stable lock of the laser away from resonance without any additional lasers.

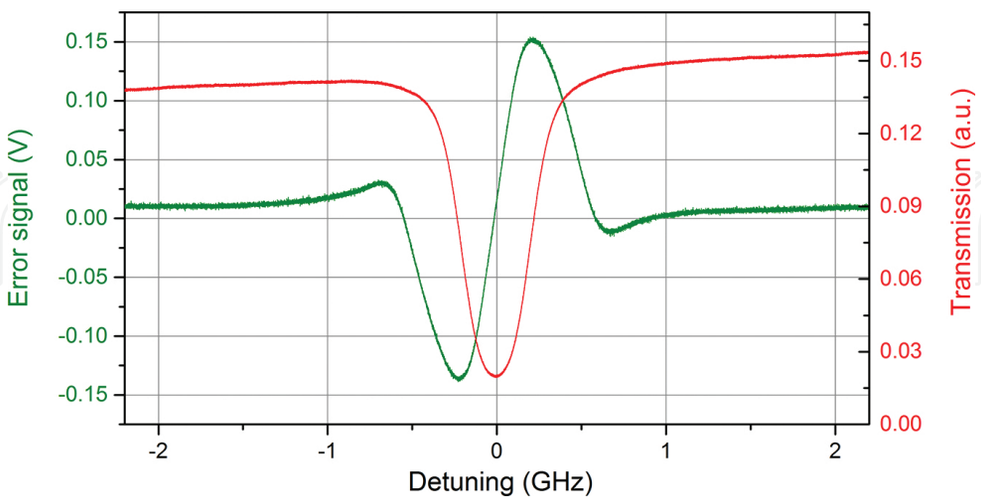

Figure 6. Experimental data from a CO_2-filled hollow-core fiber of length 10 m. The figure was adapted from [17].

To characterize the frequency stability of a system, a quantity called the Allan deviation is typically used. The Allan deviation gives information about how well the system averages out

noise over time and the type of noise present at different time scales. For the system in [17], the Allan deviation of the locked laser is shown in **Figure 7**.

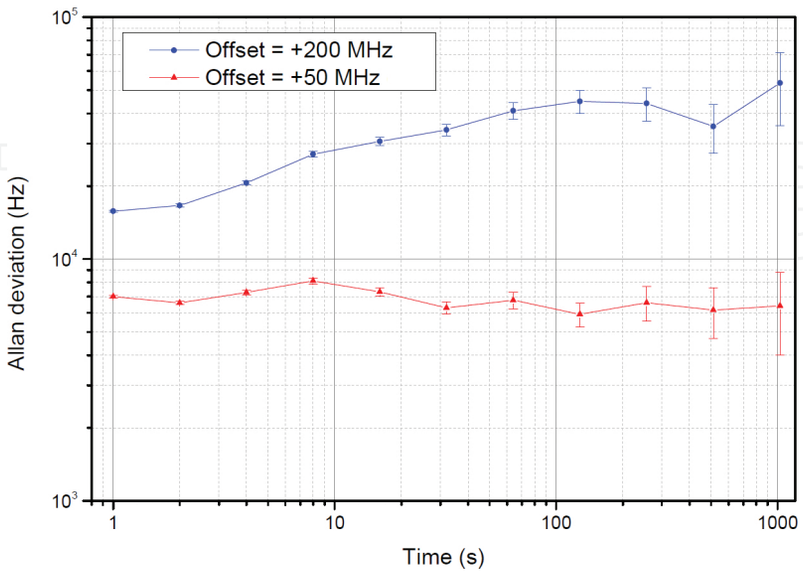

Figure 7. The Allan deviation for the locked laser system at two different offset frequencies in [17].

Here, the laser frequency stability at two different offset frequencies was measured. The figure shows that smaller offset frequency demonstrates better stability (lower Allan deviation) and that the frequency stability is dominated by flicker noise (1/*f*-type noise). This can be seen from the fact that the Allan deviation does not decrease over time. For white noise, the Allan deviation decreases as $t^{-1/2}$, where t is the time. Even with the presence of flicker noise, the level of stability here is better than 10 kHz for the low-frequency offset (50 MHz) until at least 1000 s integration time. The typical duration of the LIDAR measurement is only on the order of 10 seconds, so this stability is more than sufficient to meet the requirements.

Thus, in the study of Westergaard et al. [17], a hollow-core fiber has successfully been used for molecular spectroscopy applied to frequency stabilization of a DFB laser with the aim of satellite-based DIAL measurements.

4. Raman spectroscopy

Raman spectroscopy is a versatile technique that finds applications in physics, chemistry, biology, and in a number of different industrial areas. Raman spectroscopy typically explores transitions between motional states in molecules that have a unique energy spectrum for each molecule—a "fingerprint"—which therefore allows identification of that molecule [22].

Raman scattering is a weak process that requires high optical intensity in the excitation beam to take place. This places some limitations on the laser sources and the damage threshold of

the sample under test. Traditionally, the signal from the Raman scattering process has been obtained via a spontaneous process. The principle of the process is illustrated in **Figure 8**.

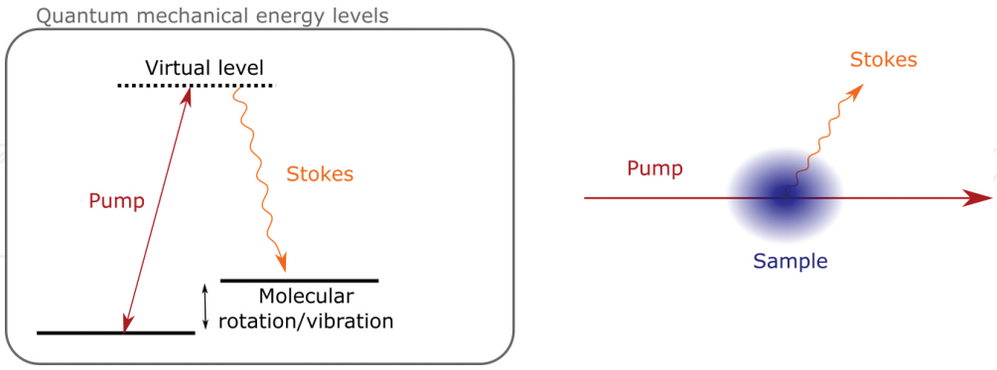

Figure 8. Spontaneous Raman scattering. A sample of molecules is excited by a pump laser, and when the molecules decay, a signal with lower (Stokes) or higher (anti-Stokes) energy is emitted from the sample in an arbitrary direction.

Here, a molecular sample is excited with a powerful pump laser to a virtual level; something which is allowed by quantum mechanics—but not very likely to happen for any given pump photon, which is why a powerful laser with a large number of photons is used. After the excitation, the molecules quickly decay to a real level, which typically is excited motionally (i.e., with more rotational or vibrational energy) with respect to the initial state.

In the decay process, the molecule emits a photon corresponding to the energy difference between the virtual level and the excited motional level. This photon contains information about the motional energy levels of the molecule, thus providing the spectroscopic fingerprint of the technique. When the level to which the molecules decay has a higher energy than the initial level (as illustrated in **Figure 8**), the emitted radiation is known as the Stokes signal. If the initial level has a higher energy, the radiation is called the anti-Stokes signal.

To achieve a larger Raman signal, a different approach can be applied, where the Raman transition is stimulated coherently using two different laser sources at the same time, with the

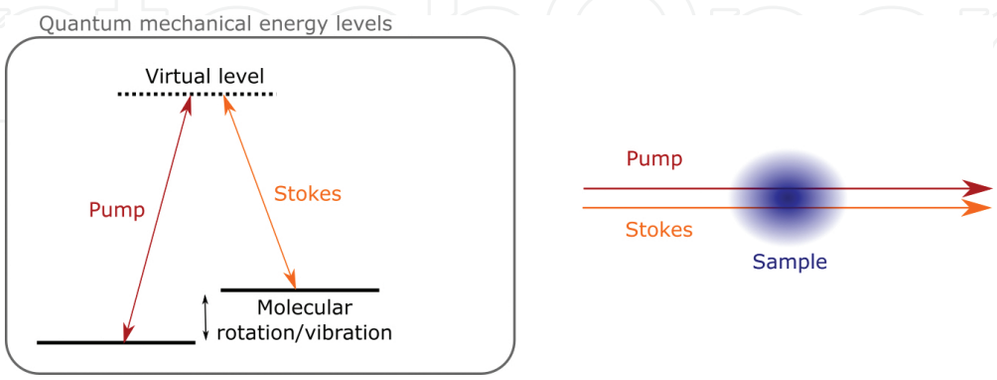

Figure 9. Stimulated Raman scattering. Here, two lasers are used to stimulate the Raman transition. The two laser beams must overlap spatially for the process to take place. Here, they are displaced slightly for clarity.

frequency difference between the two lasers corresponding to the energy difference between the two molecular levels involved in the Raman transition [22]. The situation is illustrated in **Figure 9**.

Stimulating the Raman transition in this way instead of relying on a spontaneous process has several advantages. First of all, it provides orders of magnitude larger signal [23] and makes it possible to observe the Raman signal with continuous-wave (CW) lasers with moderate (sub-Watt) optical power, which otherwise for spontaneous excitation would require Watt levels of CW power in the best case [24, 25]. Secondly, when the Raman process takes place, photons are effectively transferred from one laser beam to the other. Therefore, the signal is contained in a laser beam with a well-defined direction, in contrast to the spontaneous case where the Stokes radiation is emitted in an arbitrary direction, and the collection of the stimulated signal can be much more effective.

When the frequency difference between the two lasers matches that of an allowed Raman transition, the pump laser (typically the high-frequency laser) will be depleted, while the probe laser (typically the low-frequency laser) will experience a gain in intensity. As opposed to spontaneous scattering, which is proportional to only the pump intensity, the stimulated Raman signal is proportional to the product of the pump and probe intensity,

$$\delta I\left(\nu_{probe}\right) \propto I\left(\nu_{pump}\right) I\left(\nu_{probe}\right).$$

This proportionality gives the possibility of boosting the signal by many orders of magnitude.

By containing molecules inside a hollow-core fiber, the Raman signal is increased even further. This was first achieved around 15 years ago [23, 26]. The intrafiber interaction ensures high intensity between the light and the molecules over a long distance. It has been shown that HC-PCFs are very efficient for enhancing the Raman signals for both spontaneous [24, 27] and stimulated Raman transitions [23, 28, 29].

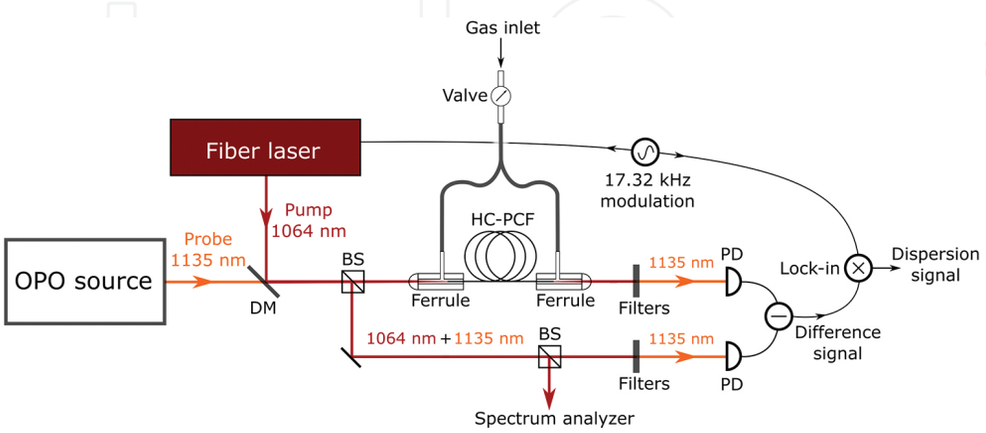

Figure 10. The setup in [29] for differential detection of stimulated Raman scattering. DM: dichroic mirror, PD: photo diode, BS: beam splitter, OPO: optical parametric oscillator.

Most recently, in [29], measurements were performed on the ortho-$S_0(1)$ transition of molecular hydrogen at 587 cm^{-1}, which is the most intense rotational line at room temperature for low wavenumbers. For a pump wavelength of 1064 nm, the Raman transition corresponds to probe (Stokes) radiation at 1135 nm. The pump light at 1064 nm was obtained from a commercial fiber laser and the light at 1135 nm was generated via a nonlinear process in a crystal—so-called optical parametric oscillator (OPO). The signal-to-noise ratio (SNR) can be further enhanced by using modulation detection [28, 29], where the pump laser is frequency modulated and this modulation is transferred to the probe laser via the Raman transition and demodulated with a lock-in amplifier giving the Raman signal. In [29], the setup was further improved by employing differential measurement detection of the probe laser, while suppressing the pump laser (see **Figure 10**). With this technique, any classical noise in the probe beam can be rejected, thus enhancing the SNR of the Raman signals. This resulted in spectroscopic data such as shown in **Figure 11**. Here, the Raman transition is probed with high sensitivity; the achieved SNR was around 1600 using only around 200 mW and 2 mW of optical power in the pump and probe laser, respectively, and a H_2 pressure of 867 hPa in 4.5 m of HC-PCF. Using two spectrally narrow light sources (such as the two lasers used here) additionally allows a for spectral resolution of features of Raman transitions down to around 5 MHz or 1.6×10^{-4} cm^{-1}, provided there are no other broadening mechanisms (which there typically are at room temperature, however, as described in Section 3.1).

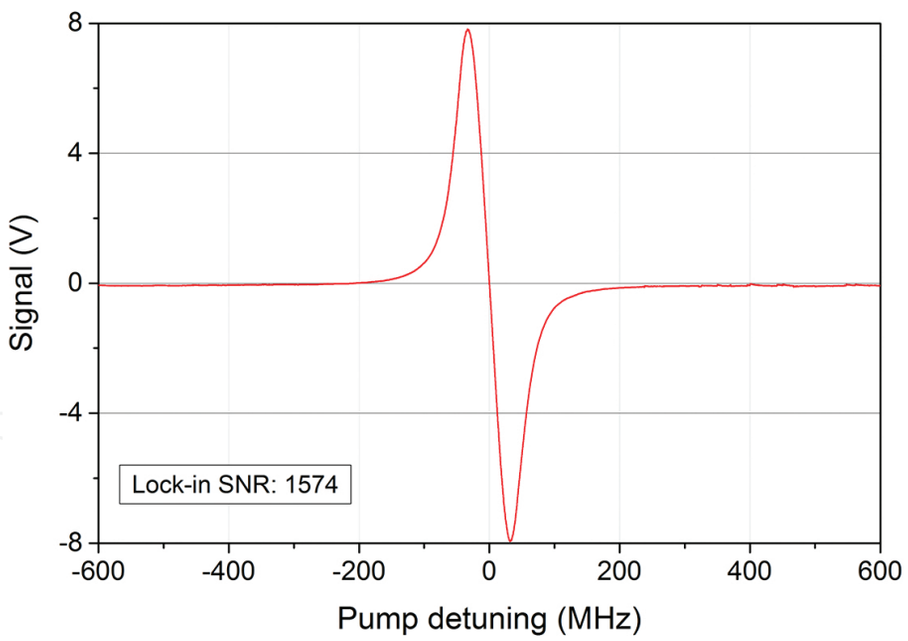

Figure 11. The signal from H_2 with around 2 mW of power in the 1135 nm (probe) laser and 200 mW in the 1064 nm (pump) laser. The Raman transition is detected using a lock-in technique, where the phase quadrature is recorded giving a dispersion-shaped curve instead of the usual absorption curve when the pump laser frequency is scanned across the Raman transition.

The measurements presented in [29] demonstrate that the use of a HC-PCF for enhancing the Raman signal makes it possible to achieve much higher SNR than without the hollow-core

fiber and in principle the system is able to measure Raman transitions with only a few mW of power in the pump and probe beams at ambient pressure with a high spectral resolution.

Author details

Philip G. Westergaard

Address all correspondence to: pgw@dfm.dk

Danish Fundamental Metrology (DFM), Lyngby, Denmark

References

[1] F. P. Kapron, D. B. Keck and R. D. Maurer, "Radiation losses in glass optical waveguides," *Applied Physics Letters,* vol. 17, p. 423, 1970.

[2] P. Russell, "Photonic crystal fibers," *Science,* vol. 299, pp. 358–362, 2003.

[3] R. F. Cregan, B. J. Mangan, J. C. Knight, T. Birks, P. Russell, P. J. Roberts and D. C. Allan, "Single-mode photonic band gap guidance of light in air," *Science,* vol. 285, pp. 1537–1539, 1999.

[4] M. Triches, M. Michieletto, J. Hald, J. Lyngsø, J. Lægsgaard and O. Bang, "Optical frequency standard using acetylene-filled hollow-core photonic crystal fibers," *Optics Express,* vol. 23, pp. 11227–11241, 2015.

[5] R. Thapa, K. Knabe, K. L. Corwin and B. R. Washburn, "Arc fusion splicing of hollow-core photonic bandgap fibers for gas-filled fiber cells.," *Optics Express,* vol. 14, no. 21, pp. 9576–9583, 2006.

[6] P. S. Light, F. Couny and F. Benabid, "Low optical insertion-loss and vacuum-pressure all-fiber acetylene cell based on hollow-core photonic crystal fiber," *Optics Letters,* vol. 31, no. 17, pp. 2538–2540, 2006.

[7] K. Knabe, "Using saturated absorption spectroscopy on acetylene-filled hollow-core fibers for absolute frequency measurements," Ph.D. thesis, Kansas State University, 2010.

[8] F. Couny, F. Benabid and P. Light, "Reduction of Fresnel back-reflection at splice interface between hollow core PCF and single-mode fiber," *IEEE Photonics Technology Letters,* vol. 19, no. 13, pp. 1020–1022, 2007.

[9] P. Marty, J. Morel and T. Feurer, "All-fiber multi-purpose gas cells and their applications in spectroscopy," *Journal of Lightwave Technology,* vol. 28, no. 8, pp. 1236–1240, 2010.

[10] P. J. Meras, I. Y. Poberezhskiy, D. H. Chang, J. Levin and G. D. Spiers, "Laser frequency stabilization for coherent lidar applications using novel all-fiber gas reference cell fabrication technique," in *24th International Laser Radar Conference (ILRC)*, Boulder, Colorado, 2008.

[11] M. Triches, A. Brusch and J. Hald, "Portable optical frequency standard based on sealed gas-filled hollow-core fiber using a novel encapsulation technique," *Applied Physics B,* vol. 121, pp. 251–258, 2015.

[12] J. Henningsen and J. Hald, "Dynamics of gas flow in hollow core photonic bandgap fibers.," *Applied Optics,* vol. 47, no. 15, pp. 2790–2797, 2008.

[13] J. Hald, J. Henningsen and J. C. Petersen, "Spectroscopy on Slow Molecules in Hollow-Core Photonic Bandgap Fibers," Frontiers in Optics 2007 (OSA's 91st Annual Meeting / Laser Science XXIII), San Jose, USA, 2007.

[14] R. Baptist and F. Levy, "Carbon dioxide adsorption on glass," *Vacuum,* vol. 43, no. 3, pp. 213–214, 1992.

[15] L. Nielsen, "Optical line profiles for use in gas monitoring," *EMRP Eumetrispec Report D1-03-01,* 2013.

[16] G. Ehret, C. Kiemle, M. Wirth, A. Amediek, A. Fix and S. Houweling, "Space-borne remote sensing of CO2, CH4, and N2O by integrated path differential absorption lidar: a sensitivity analysis," *Applied Physics B,* vol. 90, pp. 593–608, 2008.

[17] P. G. Westergaard, J. W. Thomsen, M. Henriksen, M. Michieletto, M. Triches, J. K. Lyngsø and J. Hald, "Compact, CO2-stabilized tuneable laser at 2.05 microns," *Optics Express,* vol. 24, no. 5, pp. 4872–4880, 2016.

[18] K. Numata, J. R. Chen, S. T. Wu, J. B. Abshire and M. a. Krainak, "Frequency stabilization of distributed-feedback laser diodes at 1572 nm for lidar measurements of atmospheric carbon dioxide.," *Applied Optics,* vol. 50, no. 7, pp. 1047–1056, 2011.

[19] K. Numata, J. R. Chen and S. T. Wu, "Precision and fast wavelength tuning of a dynamically phase-locked widely-tunable laser.," *Optics Express,* vol. 20, no. 13, pp. 14234–14243, 2012.

[20] P. Meras, I. Y. Poberezhskiy, D. H. Chang and G. D. Spiers, "Frequency stabilization of a 2.05 μm laser using hollow-core fiber CO2 frequency reference cell," Proc. of SPIE vol. 7677, p. 767713, 2010.

[21] A. Lurie, F. N. Baynes, J. D. Anstie, P. S. Light, F. Benabid, T. M. Stace and A. N. Luiten, "High-performance iodine fiber frequency standard," *Optics Letters,* vol. 36, pp. 4776–4778, 2011.

[22] N. B. Colthup, L. H. Daly and S. E. Wiberley, "Introduction to infrared and Raman spectroscopy," 2nd ed., Academic Press New York, 1975.

[23] F. Benabid, J. C. Knight, G. Antonopoulos and P. S. J. Russel, "Stimulated Raman scattering in hydrogen-filled," *Science,* vol. 298, pp. 399–402, 2002.

[24] F. Couny, F. Benabid and P. S. Light, "Subwatt threshold cw Raman fiber-gas laser based on H2-filled hollowcore," *Physical Review Letters,* vol. 99, p. 143903, 2007.

[25] F. Couny, O. Carraz and F. Benabid, "Control of transient regime of stimulated Raman scattering using hollow-core PCF," *Journal of the Optical Society of America B,* vol. 26, pp. 1209–1215, 2009.

[26] F. Benabid, F. Couny, J. C. Knight, T. A. Birks and P. S. J. Russell, "Compact, stable and efficient all-fibre gas cells using hollow-core photonic crystal fibres," *Nature,* vol. 434, pp. 488–491, 2005.

[27] M. P. Buric, K. P. Chen, J. Falk and S. D. Woodruff, "Enhanced spontaneous Raman scattering and gas composition analysis using a photonic crystal fiber," *Applid Optics,* vol. 47, pp. 4255–4261, 2008.

[28] J. L. Doménech and M. Cueto, "Sensitivity enhancement in high resolution stimulated Raman spectroscopy of gases with hollow-core photonic crystal fibers," *Optics Letters,* vol. 38, p. 4074–4077, 2013.

[29] P. G. Westergaard, M. Lassen and J. C. Petersen, "Differential high-resolution stimulated CW Raman spectroscopy of hydrogen in a hollow-core fiber," *Optics Express,* vol. 23, pp. 16320–16328, 2015.

IntechOpen